Temperature inversion in a gravitationally bound plasma: the case of the solar corona

Luca Barbieri,[1,2,3,*] Lapo Casetti,[1,2,3,†] Andrea Verdini,[1,2,‡] and Simone Landi[1,2,§]

[1] *Dipartimento di Fisica e Astronomia, Università di Firenze, via G. Sansone 1, I-50019 Sesto Fiorentino, Italy*
[2] *INAF-Osservatorio Astrofisico di Arcetri, Largo Enrico Fermi 5, I-50125 Firenze, Italy*
[3] *INFN, Sezione di Firenze, via G. Sansone 1, I-50019 Sesto Fiorentino, Italy*

(Dated: submitted to Physical Review Letters on March 21, 2023; revised August 10, 2023)

The temperature of the solar atmosphere increases from thousands to millions of degrees moving from the lower layer, the chromosphere, to the outermost one, the corona, while density drops by several orders of magnitude. Such a phenomenon is called temperature inversion and how it happens is still largely unknown. We argue that temperature fluctuations in the chromosphere play a key rôle, as suggested by the study of a kinetic model of a plasma confined in a semicircular tube subjected to the gravity of the Sun and in contact with a thermostat at its feet, mimicking a coronal loop anchored in the chromosphere. Collisions are neglected in the corona, with a sharp transition to a fully collisional chromosphere. Numerical simulations and analytical calculations show that suitable fluctuations of the thermostat temperature drive the plasma towards a non-thermal stationary state with temperature and density profiles strikingly similar to those observed in the atmosphere of the Sun, suggesting this mechanism may significantly contribute to coronal heating.

Introduction. When temperature and density are anti-correlated in a stationary state, i.e., the system is hotter where it is thinner, one speaks of temperature inversion. It happens in astrophysical systems such as filaments in molecular clouds [1, 2], the Io plasma torus around Jupiter [3], the Earth's magnetosphere [4], the hot gas in some galaxy clusters [5, 6] and, notably, the solar atmosphere, which is with no doubt the most striking and thoroughly studied example (see e.g. [7] and references therein). The Sun's outermost layer, the corona, reaches temperatures above 10^6 K and lies on top of a denser and cooler (roughly 10^4 K) layer, the chromosphere, the two layers being connected by the so-called transition region, a thin interface only hundreds of kilometers wide in which temperature jumps by a factor of 50 and density drops by the same factor [8]. How this happens is still unknown and is commonly referred to as the coronal heating problem [9, 10].

Assuming local thermodynamic equilibrium, a corona can form only upon direct heating of the upper layer. The energy coming from the Sun is enough to heat the whole corona [11], bringing the problem to how to transport and dissipate energy at coronal heights. Proposed mechanisms involve release of magnetic energy stored in the corona [12–17], transmission and damping of waves generated by photospheric motions [18–20], or direct insertion of hot plasma in form of chromospheric spicules [21].

However, there are theoretical indications [22, 23] and observational evidences [24] that local thermodynamic equilibrium may not be satisfied in the transition region and in the corona. This allows for another way of obtaining temperature inversion, as first realized by Scudder [25, 26]. If the velocity distribution functions (VDFs) of electrons and ions have suprathermal tails in the chromosphere, then temperature must increase with height[27]: faster particles are able to climb higher in the Sun's gravity well and temperature increases thanks to "velocity filtration". Notably this implies no direct heating of the upper layers. Unfortunately, the model does not produce a transition region and, more importantly, non-thermal distributions in the strongly collisional chromospheric plasma are difficult to justify.

Interestingly, recent numerical studies have shown that when an isolated system governed by long-range interactions is impulsively perturbed it undergoes collisionless relaxation reaching a non-thermal stationary state with temperature inversion, whose origin can be traced back to velocity filtration [28–30]. This might explain the inverted temperature-density profiles of filaments in molecular clouds [31], but it cannot be applied as such to the coronal plasma, which is not isolated but rather in steady thermal contact with the chromosphere. However, while the VDFs of the chromospheric plasma are likely to be thermal due to collisionality, the chromosphere is a very dynamic environment showing fine-scale structures down to instruments' resolution [32, 33], and its temperature is expected to fluctuate in space and time [34, 35].

In this letter, using both numerical simulations and analytical modelling, we show that rapid temperature fluctuations in the chromosphere are able to build up a hot corona. For simplicity we model a coronal loop as a semicircular tube of collisionless plasma in thermal contact with a thermostat, the latter playing the rôle of the dynamic and collisional chromospheric plasma. The tunable part of the model is the statistics of the temperature fluctuations of the chromosphere. Temperature inversion appears as a very robust phenomenon and does not require any fine-tuning. However, matching the density and temperature values of the solar corona, and obtaining a (thick) transition region, requires a specific range of temperature fluctuations, and we briefly discuss whether

the latter might be observationally tested.

Model and numerical simulations. We consider a model of the plasma in a coronal loop made up of $N_e = N_i = 2N$ protons and electrons having mass m_i and m_e and charge $e_i = -e_e = e$. Particles are confined in a semicircular tube of length $2L$ and cross section S, and are subjected to a constant downward gravity and to an electric force which ensures charge neutrality, whose combined effect is proportional to $(m_e + m_i)/2$ [36–38]. We assume that all quantities depend only on the coordinate along the loop axis, $x \in [-L, L]$, and are symmetric with respect to the loop top located at $x = 0$. We expand the electrostatic interactions between the particles in a Fourier series and retain only the first mode, as in the Hamiltonian Mean Field model [39–41], so that each particle only feels the average effect of all the others: in the limit of large N, the dynamics is collisionless. The equations of motion read

$$m_\alpha \ddot{x}_{j,\alpha} = e_\alpha E(x_{j,\alpha}) + g\frac{m_e + m_i}{2}\sin\left(\frac{\pi x_{j,\alpha}}{2L}\right) , \quad (1)$$

where $j = 1, \ldots, 2N$ numbers the particles, $\alpha = e, i$ denotes the species, $g = GM_\odot/R_\odot^2$ is the Sun gravity, and

$$E(x) = 8\frac{|e_\alpha|}{S}N\,(q_i - q_e)\sin\left(\frac{\pi x}{L}\right) \quad (2)$$

is the self-consistent electric field [42], with

$$q_\alpha = \frac{1}{2N}\sum_{j=1}^{2N}\cos\left(\frac{\pi x_{j,\alpha}}{L}\right) . \quad (3)$$

The stratification parameters q_α in Eq. (3) are such that $q_\alpha = 0$ corresponds to a uniform distribution throughout the loop and $q_\alpha = -1$ (resp. 1) to a distribution concentrated in $x = \pm L$ (resp. 0); $q_i - q_e$ appearing in Eq. (2) measures the charge imbalance. The anchoring of the loop feet to the high chromosphere is modeled by coupling the coronal plasma to a thermostat at $x = \pm L$: when a particle reaches the boundary, it is reinjected into the loop with a random velocity consistent with the flux from a thermal distribution at the temperature of the thermostat [43–45]. Once written using dimensionless variables, the equations of motion depend only on three parameters: the mass ratio, $M = m_i/m_e$, and the strengths of the interactions, C and $\tilde{g}$, expressed as the electrostatic and gravitational energy, respectively, normalized to the thermal energy,

$$C = \frac{8ne^2L^2}{\pi k_B T_0} \text{ and } \tilde{g} = \frac{gL(m_i + m_e)}{2\pi k_B T_0} , \quad (4)$$

where n is the the average number density of each species, k_B is the Boltzmann constant and $T_0 = 10^4$ K is the reference temperature of the thermostat and our unit of temperature.

Starting with the plasma in thermal equilibrium at the initial thermostat's temperature $T = 1$ (in our units), the latter is allowed to vary so as to mimic the dynamic nature of the chromosphere. After a waiting time t_w we increase the thermostat temperature by a quantity ΔT, we keep the thermostat at $T = 1 + \Delta T$ for a time τ, and then we switch back to $T = 1$. These steps are iterated for the whole duration of the simulation run, drawing the values of t_w and ΔT from two exponential distributions,

$$\eta(t_w) = \frac{1}{\langle t_w\rangle}e^{-\frac{t_w}{\langle t_w\rangle}} \text{ and } \gamma(\Delta T) = \frac{1}{T_p}e^{-\frac{\Delta T}{T_p}} . \quad (5)$$

The physical idea is that the chromospheric temperature fluctuates due to random heating events, among which those producing a larger ΔT are less likely to happen. We observe that when both t_w and τ are sufficiently small, and in particular smaller than the relaxation times to equilibrium, the plasma in the loop is kept away from the initial thermal state, never relaxes to a thermal distribution with $T > 1$, but it rather attains a nonequilibrium stationary state, with non-thermal distribution functions and inverted temperature-density profiles.

Simulation results. We now focus on the case of a coronal loop with average number density $n = 2.5\times10^9$ cm^{-3} and half-length $L = \pi \times 10^4$ km, so that $\tilde{g} = 16.64$. For the mass ratio we chose the realistic value $M = 1836$. A realistic value of the parameter $C \approx 10^{22}$ implies very fast plasma oscillations and prohibitively small integration time steps ($\approx 1/\sqrt{C}$) to reliably simulate the dynamics. However, we checked that in the stationary state the temperature and density profiles as well as the VDFs do not depend on the value of C, which only affects amplitude and frequency of the oscillations around the means. Therefore, we arbitrarily chose $C = 400$ to have oscillations with periodicity larger than the thermostat timescale (see below), meaning that our simulated particles have a much smaller charge than in the real world. The simulations were performed using $N \approx 2.1 \times 10^6$, $\tau = 8 \times 10^{-4}$, $\langle t_w\rangle = 4 \times 10^{-2}$, and $T_p = 90$, i.e., 9×10^5 K in physical units [46]. Together with the choice of $T_0 = 10^4$ K, these values imply an average temperature $T_b \approx 1.2 \times 10^4$ K at the base of the loop (see below). This sets the base at a height $z_b \approx 2 \times 10^3$ km above the chromosphere, where the transition region begins, and the top of the loop at $z_t \approx 2.2 \times 10^4$ km, well into the corona.

In the top panel of Fig. 1 we report the time evolution of the kinetic energies per particle

$$K_\alpha = \frac{1}{2N}\sum_{j=1}^{2N}\frac{p_{j,\alpha}^2}{2M_\alpha} , \quad (6)$$

where $p_{j,\alpha}$ is the dimensionless momentum of the j-th particle of species α, with $M_e = 1$ and $M_i = M$; in the bottom panel the stratification parameters q_e and q_i defined in Eq. (3) are reported, again as a function

of time. After a transient, a stationary state is reached where all these quantities fluctuate around constant values, the transient being longer and the amplitude of the fluctuations smaller for the ions, as expected due to their larger mass. The initial value $q_i = q_e \approx -0.99$ corresponds to the stratification of an isothermal atmosphere at $T = 1$. In the stationary state, which is not a thermal equilibrium state as we shall see in the following, a smaller value is obtained, $q_i \approx q_e \approx -0.94$, indicating a slightly milder stratification.

In Fig. 2 we report the temperature and density profiles along the loop, obtained by time-averaging in the stationary state. To make the comparison with the known profiles of the solar atmosphere easier, we report the results in physical units as a function of the height z above the chromosphere (temperatures in K, densities in cm^{-3}, height in km). Temperature inversion is clearly visible, as well as the presence of a transition region: indeed, there is a sharp increase (resp. decrease) of the temperature (resp. density) roughly between $z = 2 \times 10^3$ and $z = 5 \times 10^3$ km, with a jump from 1.2×10^4 to 6×10^5 K while density drops by two orders of magnitude, followed by a gentler change of both quantities. Both the values of T and n and the shape of the curves are strikingly similar to those of the Sun atmosphere (see e.g. [7, 8]), but for the fact that the transition region in our model is larger than in the real case, that is, roughly 3×10^3 km against less than 2×10^2 km.

Theory. The numerical results can be reproduced and explained computing the distribution functions (DFs) $f_\alpha(\vartheta, p)$ of ions and electrons in the nonequilibrium stationary state (ϑ is the dimensionless position). To this end, we first consider the time averaged incoming flux of energy at the feet of the loop, i.e., at $\vartheta = \pm\pi$, which can be written for each species as $J_{IN,\alpha} = \langle J_{T(t),\alpha} \rangle_t$, where

$$J_{\zeta,\alpha} = \int_0^{+\infty} dp \, \frac{p}{\zeta M_\alpha} \, e^{-\frac{p^2}{2\zeta M_\alpha}} \tag{7}$$

is the flux when the thermostat is at temperature ζ. To explicitly compute $J_{IN,\alpha}$ we replace time averages with averages over the probability distributions of waiting times and of thermostat temperatures, obtaining

$$J_{IN,\alpha} = (1 - A) J_{1,\alpha} + A \langle J_{1+\Delta T,\alpha} \rangle_\gamma \, , \tag{8}$$

where $A = \tau / (\tau + \langle t_w \rangle_\eta)$ and $\langle \cdot \rangle_\gamma$ and $\langle \cdot \rangle_\eta$ stand for averages over the distributions γ and η given in Eq. (5). In our model the plasma in the loop is collisionless, so that f_α obeys the Vlasov equation and in the stationary state it depends on ϑ and p only via the single-particle Hamiltonian

$$H_\alpha(\vartheta, p) = \frac{p^2}{2M_\alpha} + 2\tilde{g} \cos\left(\frac{\vartheta}{2}\right) \, , \tag{9}$$

as implied by the Jeans theorem. Note that also an electrostatic interaction term proportional to the effective electric field should be present in Eq. (9), but it can be proved that it vanishes in the stationary state [47]. The DF at $\vartheta = \pm\pi$ is fixed imposing equality of the incoming and outgoing fluxes at the feet of the loop, that is, $J_{IN,\alpha} = J_{OUT,\alpha}$, with

$$J_{OUT,\alpha} = \int_{-\infty}^{0} dp \, p \, f_\alpha(\pm\pi, p) \, . \tag{10}$$

The result for $f_\alpha(\vartheta, p)$ in the stationary state is [48]

$$\begin{aligned} f_\alpha(\vartheta, p) = \mathcal{N} \Bigg[& (1 - A) \frac{e^{-H_\alpha(\vartheta,p)}}{M_\alpha} \\ & + A \int_0^{+\infty} d\zeta \, \gamma(\zeta) \, \frac{e^{-\frac{H_\alpha(\vartheta,p)}{1+\zeta}}}{(1+\zeta) M_\alpha} \Bigg] \, , \end{aligned} \tag{11}$$

where $\mathcal{N}$ is a normalization constant fixed by imposing $\int_{-\infty}^{+\infty} dp \int_{-\pi}^{\pi} d\vartheta \, f_\alpha(\vartheta, p) = 1$. The interpretation of Eq. (11) is rather transparent: the stationary DF is given by a thermal distribution at temperature $T = 1$ plus a non-thermal contribution arising from the average of thermal distributions at $T = 1 + \zeta$ over the probability distribution $\gamma(\zeta)$ of the temperature fluctuations. The weight of the non-thermal contribution is proportional to A, the fraction of time in which the thermostat is not at temperature $T = 1$. The thermal population dominates at small heights z, and is depressed by the gravity term in H_α when increasing z; conversely, the non-thermal contribution becomes more and more relevant at larger z due to velocity filtration, because faster particles can climb higher in the potential well, showing up as suprathermal tails in the distribution.

This is shown in Fig. 3 where the VDFs of electrons normalized by the density are plotted at three increasing heights, $z = 2.3,\ 3.9,\ 11 \times 10^3$ km from bottom to top, corresponding to the base of the transition region, the middle transition region, and the corona, respectively. Red, blue and green curves are obtained from the simulation, while grey curves are the theoretical predictions of Eq. (11). Note that VDFs are reported as functions of the signed kinetic energy $\mathrm{sign}(p)\, p^2/2$ in a semilogarithmic scale, so that a thermal distribution (a Gaussian) appears as a triangle symmetric about zero. The VDFs are always composed of a thermal core at small velocities plus a suprathermal tail at larger velocities. As height increases, the thermal core progressively shrinks and almost disappears in the corona, where the VDF is basically suprathermal.

These VDFs explain the shape of the temperature and density profiles reported in Fig. 2, where the grey curves are the theoretical prediction obtained with Eq. (11). The sharp temperature rise in the transition region (and density decrease) is caused by the dramatic change in the shape of the VDF that passes from being nearly thermal to almost completely suprathermal. Once coronal heights are reached, totally nonthermal VDFs produce a gentler

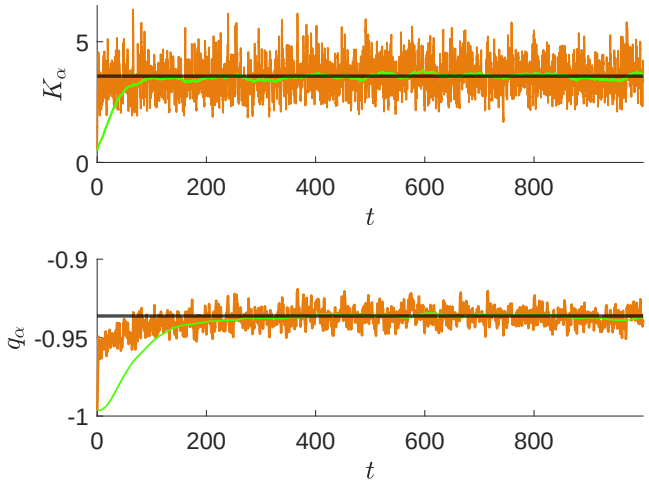

FIG. 1. Kinetic energies (top) and stratification parameters (bottom) of ions and electrons in green and orange, respectively, as a function of time. The black horizontal lines are the theoretical stationary values predicted using Eq. (11).

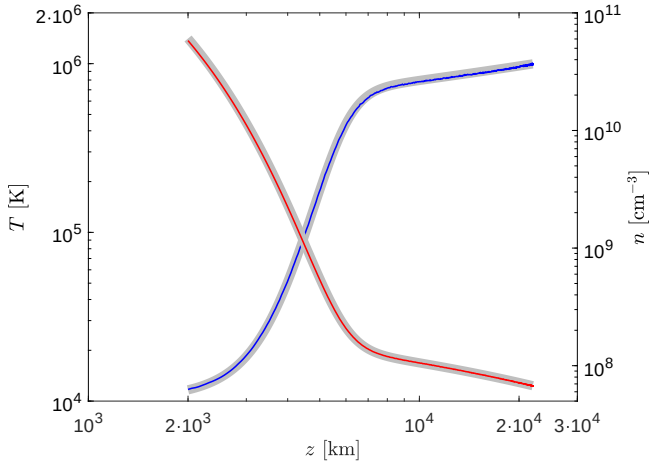

FIG. 2. Electron density (red) and temperature (blue) as a function of the height above the photosphere, obtained in a numerical simulation with parameters corresponding to the solar atmosphere (see text). The thick grey lines are the theoretical profiles computed using Eq. (11).

variation of temperature and density, similar to the case described in [25, 26]. For completeness, the stationary values of the kinetic energies and stratification parameter computed using Eq. (11) are drawn with black horizontal lines in Fig. 1. Theoretical results show remarkable agreement with numerical ones in all the figures.

Discussion. We have presented a very simple model of the solar atmosphere, where the collisonless coronal plasma is in steady contact with a thermostat mimicking a completely collisional chromosphere. The analyical and numerical results consistently show that in response to short-lived increments of the chromospheric temperature,

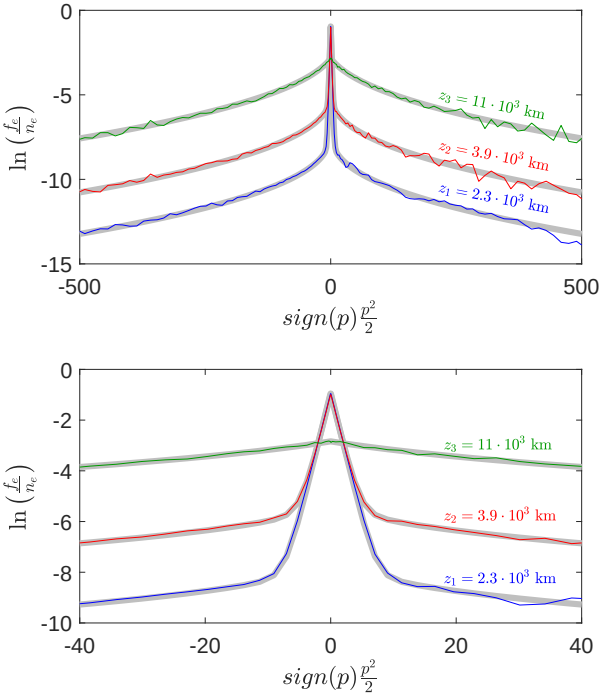

FIG. 3. Electron VDFs (color curves) normalized by the electron densities as a function of the signed kinetic energy, at different heights (see labels). Theoretical VDFs computed from Eq. (11) are plotted as thick grey lines. In the bottom panel, a magnification of the central region of the same VDFs is shown to appreciate the disappearance of the Gaussian profile.

suprathermal tails in the VDFs naturally form and gravitational filtering causes a sharp temperature rise and density decrease in the above atmosphere, consisting of a (thicker than observed) transition region, followed by an extended corona at roughly 10^6 K.

Suprathermal electrons, along with a thermal population, are measured *in situ* in the solar wind [49–51]. Their presence in the transition region [24] or in flaring regions [52] is also compatible with remote sensing observations of non-thermal line widths, but direct detection is still challenging. Our model supports the formation of a nonthermal population already at the base of the corona, thus favouring the formation of the solar wind by gravitational filtering as in exospheric models [53–57].

Fundamental in achieving temperature inversion is that the coronal plasma is in a nonequilibrium stationary state. This requires the chromosphere to maintain any given temperature for intervals much shorter than the relaxation time of electrons in the corona, t_R, which in our model is expected to be the shortest between the sound travel time and the free fall time, that is, roughly 10 s for the parameters we considered above. To reach temperatures around 10^6 K in the corona while keeping temper-

atures around 10^4 K at the base of the transition region, the mean of chromospheric temperature increments must be as large as the coronal temperature, i.e., $T_p \approx 10^6$ K, but the ratio between their duration τ and the typical waiting time $\langle t_w \rangle$ between them must be small, so that $\tau \ll \langle t_w \rangle \ll t_R$.

Short-lived, intense, and small-scale brightenings are routinely observed on the Sun [34, 58–61]. The so-called campfires, recently observed in extreme UV imaging by Solar Orbiter, have temperatures of $\approx 10^6$ K, while explosive events appearing in Hα line widths have smaller temperatures, around 2×10^5 K [59], but are ten times more frequent. This trend is compatible with the exponential distribution of temperature increments we assumed. However, current measurements have a temporal resolution which is at best of a few seconds, so that temperature increments able to form a corona according to our model remain unresolved. Anyhow, even in the case of unresolved events, a given temperature measurement brings a footprint of the underlying event distribution. For instance, assuming $\langle t_w \rangle \approx 1$ s, with $\tau \approx 0.1$ s our model would predict an average temperature $T \approx 2 \times 10^4$ K at the top of the chromosphere, which is not observed; however, if $\tau \approx 1/50$ s we get $T \approx 1.2 \times 10^4$ K, as in the case we have shown in Fig. 2. This is consistent with ALMA observations of brightness temperatures as large as 1.2×10^4 K [62], with measurements at 2 s cadence. A possible physical mechanism at work is magnetic reconnection in the low atmosphere, as suggested by recent observations [63, 64].

The main result in this letter is that the average temperature profile of the solar atmosphere can be obtained keeping the coronal plasma in thermal contact with the chromosphere, without direct heating. At variance with previous results based on velocity filtration, a transition region shows up, and non-thermal chromospheric VDFs are not needed: a corona can be formed out of a collisional, but dynamic, chromosphere. The simplicity of the model makes it analytically solvable and allows to investigate the effects of a single mechanism without having to disentangle it from other ones. Clearly, this does not exclude that also other mechanisms contribute to coronal heating.

Potentially important physics is neglected in the model presented here, e.g., radiation losses, collisions in the corona, and magnetic fields. Although a detailed discussion of these effects is beyond the scope of this work, let us briefly address them. In our model, energy is transported in the corona by the particles' stream, and is exchanged with the thermostat on a timescale of the order of the crossing time of the loop, which is less than a minute and much smaller than the radiation timescale (around 30 m, see e.g. [65–67]), so that energy losses due to radiation can be safely neglected in our model. Moreover, radiation losses would not change the picture, because in the nonequilibrium state a heat flux towards the radiating region would set in and restore the temperature profile [22, 43, 68]. Collisions between particles will surely occur in the corona. Relaxing the drastic approximation of a fully collisional chromosphere in contact with a completely collisionless coronal plasma would imply a much more complicated description. However, due to the nature of Coulomb collisions, whose cross section strongly depends on the particles' energy, the mean free path of a particle with velocity v is proportional to v^4. Therefore, we expect that only "cold" particles would be heavily affected by collisions: the VDFs would become closer to thermal at small energies, while non-thermal features related to the "hot" particles, which are the ones selected by gravitational filtering and can then reach coronal heights, would not be erased by collisions [22, 43]. Velocity filtration is then expected to become more efficient in presence of some degree of collisionality: the latter effect, together with particle confinement by magnetic lines, may result in a transition region sharper than the one obtained here and closer to the observed one.

The mechanism producing temperature inversion in the solar corona in our model is very general, and might be relevant to other systems where hot coronae are thought to be present, e.g., stars other than the Sun, but also active galactic nuclei. Moreover, our results show how peculiar behaviors due the absence of thermal equilibrium allow to explain seemingly paradoxical phenomena without invoking *ad hoc* mechanisms.

We thank G. Cauzzi, P. Di Cintio, and E. Papini for very useful discussions. We acknowledge partial financial support from the MIUR-PRIN2017 project *Coarse-grained description for non-equilibrium systems and transport phenomena (CO-NEST)* n. 201798CZL and from Fondazione Cassa di Risparmio di Firenze under the projects *HIPERCRHEL* and *THE SWITCH*.

* Corresponding author. E-mail: luca.barbieri@unifi.it
† E-mail: lapo.casetti@unifi.it
‡ E-mail: andrea.verdini@unifi.it
§ E-mail: simone.landi@unifi.it

[1] D. Arzoumanian, P. André, P. Didelon, V. Konyves, N. Schneider, A. Menoshchikov, T. Sousbie, A. Zavagno, S. Bontemps, J. Di Francesco, M. Griffin, M. Hennemann, T. Hill, J. Kirk, P. Martin, V. Minier, S. Molinari, F. Motte, N. Peretto, S. Pezzuto, L. Spinoglio, D. Ward-Thompson, G. White, and C. D. Wilson, Astronomy and Astrophysics **529**, L6 (2011).
[2] C. Toci and D. Galli, Monthly Notices of the Royal Astronomical Society **446**, 2110 (2015).
[3] N. Meyer-Vernet, M. Moncuquet, and S. Hoang, Icarus **116**, 202 (1995).
[4] X. Ma, K. Nykyri, A. Dimmock, and C. Chu, Journal of Geophysical Research: Space Physics **125**, e2020JA028209 (2020).

[5] A. Baldi, S. Ettori, P. Mazzotta, P. Tozzi, and S. Borgani, Astrophys. J. **666**, 835 (2007).
[6] M. W. Wise, B. R. McNamara, and S. S. Murray, Astrophys. J. **601**, 184 (2004).
[7] L. Golub and J. M. Pasachoff, *The Solar Corona*, 2nd ed. (Cambridge University Press, Cambridge, 2009).
[8] Yang, S. H., Zhang, J., Jin, C. L., Li, L. P., and Duan, H. Y., Astron. Astrophys. **501**, 745 (2009).
[9] J. A. Klimchuk, Solar Physics **234**, 41 (2006).
[10] C. E. Parnell and I. De Moortel, Philosophical Transactions of the Royal Society of London Series A **370**, 3217 (2012).
[11] G. L. Withbroe, in *Saas-Fee Advanced Course 11: Activity and Outer Atmosphere of the Sun and Stars*, edited by F. Praderie, D. S. Spicer, and G. L. Withbroe (1981) p. 1.
[12] E. N. Parker, Astrophysical Journal **174**, 499 (1972).
[13] P. Dmitruk and D. O. Gomez, Astrophysical Journal Letters v.484 **484**, L83 (1997).
[14] B. V. Gudiksen and Å. Nordlund, Astrophys. J. **618**, 1020 (2005).
[15] F. Rappazzo, M. Velli, G. Einaudi, and R. B. Dahlburg, Astrophys. J. **677**, 1348 (2008).
[16] A. F. Rappazzo and E. N. Parker, Astrophys. J. Lett. **773**, L2 (2013).
[17] A. L. Wilmot-Smith, Philosophical Transactions of the Royal Society of London Series A **373**, 20140265 (2015).
[18] J. Heyvaerts and E. R. Priest, Astron. Astrophys. **117**, 220 (1983).
[19] J. A. Ionson, Astrophys. J. **226**, 650 (1978).
[20] T. A. Howson, I. De Moortel, and J. Reid, Astron. Astrophys. **636**, A40 (2020).
[21] B. D. Pontieu, S. W. Mcintosh, M. Carlsson, . H. Viggo H, T. D. Tarbell, P. Boerner, J. Martinez-Sykora, C. J. Schrijver, and A. M. Title, Science **331**, 55 (2011).
[22] E. C. Shoub, Astrophys. J. **266**, 339 (1983).
[23] R. Esser and R. J. Edgar, Astrophys. J. Lett. **532**, L71 (2000).
[24] J. Dudík, V. Polito, E. Dzifčáková, G. Del Zanna, and P. Testa, Astrophys. J. **842**, 19 (2017).
[25] J. D. Scudder, Astrophys. J. **398**, 299 (1992).
[26] J. D. Scudder, Astrophys. J. **398**, 319 (1992).
[27] Kappa functions [69] were employed in Refs. [25, 26] to solve the problem analytically.
[28] L. Casetti and S. Gupta, European Physical Journal B **87**, 91 (2014).
[29] T. N. Teles, S. Gupta, P. Di Cintio, and L. Casetti, Phys. Rev. E **92**, 020101 (2015).
[30] S. Gupta and L. Casetti, New Journal of Physics **18**, 103051 (2016).
[31] P. Di Cintio, S. Gupta, and L. Casetti, Monthly Notices of the Royal Astronomical Society **475**, 1137 (2017).
[32] G. Cauzzi, K. Reardon, R. J. Rutten, A. Tritschler, and H. Uitenbroek, Astron. Astrophys. **503**, 577 (2009).
[33] I. Ermolli, F. Giorgi, M. Murabito, M. Stangalini, V. Guido, M. Molinaro, P. Romano, S. L. Guglielmino, G. Viavattene, G. Cauzzi, S. Criscuoli, K. P. Reardon, and A. Tritschler, Astron. Astrophys. **661**, A74 (2022).
[34] H. Peter, H. Tian, W. Curdt, D. Schmit, D. Innes, B. De Pontieu, J. Lemen, A. Title, P. Boerner, N. Hurlburt, T. D. Tarbell, J. P. Wuelser, J. Martínez-Sykora, L. Kleint, L. Golub, S. McKillop, K. K. Reeves, S. Saar, P. Testa, C. Kankelborg, S. Jaeggli, M. Carlsson, and V. Hansteen, Science **346**, 1255726 (2014).
[35] V. Hansteen, B. De Pontieu, M. Carlsson, J. Lemen, A. Title, P. Boerner, N. Hurlburt, T. D. Tarbell, J. P. Wuelser, T. M. D. Pereira, E. E. De Luca, L. Golub, S. McKillop, K. Reeves, S. Saar, P. Testa, H. Tian, C. Kankelborg, S. Jaeggli, L. Kleint, and J. Martínez-Sykora, Science **346**, 1255757 (2014).
[36] A. Pannekoek, Bull. Astr. Inst. Netherlandd **1**, 107 (1922).
[37] S. Rosseland, MNRAS **84**, 720 (1924).
[38] G. Belmont, R. Grappin, F. Mottez, F. Pantellini, and G. Pelletier, *Collisionless Plasmas in Astrophysics* (Wiley, 2013).
[39] M. Antoni and S. Ruffo, Phys. Rev. E **52**, 2361 (1995).
[40] G. Giachetti and L. Casetti, Journal of Statistical Mechanics: Theory and Experiment **4**, 043201 (2019).
[41] P. H. Chavanis, J. Vatteville, and F. Bouchet, The European Physical Journal B **46**, 61 (2005).
[42] We use electrostatic cgs units.
[43] S. Landi and F. G. E. Pantellini, Astron. Astrophys. **372**, 686 (2001).
[44] S. Lepri, G. Ciraolo, P. Di Cintio, J. Gunn, and R. Livi, Phys. Rev. Res. **3**, 013207 (2021).
[45] R. Tehver, F. Toigo, J. Koplik, and J. R. Banavar, Phys. Rev. E **57**, R17 (1998).
[46] We used a fourth-order symplectic algorithm [70] to integrate the equations of motion, with timestep $\delta t = 10^{-4}$.
[47] L. Barbieri, L. Casetti, A. Verdini, S. Landi, P. Di Cintio, and E. Papini, in preparation (2023).
[48] A full derivation will be given in [47].
[49] W. G. Pilipp, K.-H. Muehlhaeuser, H. Miggenrieder, M. D. Montgomery, and H. Rosenbauer, J. Geophys. Res. (Space Physics) **92**, 1075 (1987).
[50] J. S. Halekas, P. Whittlesey, D. E. Larson, D. McGinnis, M. Maksimovic, M. Berthomier, J. C. Kasper, A. W. Case, K. E. Korreck, M. L. Stevens, K. G. Klein, S. D. Bale, R. J. MacDowall, M. P. Pulupa, D. M. Malaspina, K. Goetz, and P. R. Harvey, Astrophys. J. Supl. Series **246**, 22 (2020).
[51] M. Maksimovic, S. D. Bale, L. Berčič, J. W. Bonnell, A. W. Case, T. Dudok de Wit, K. Goetz, J. S. Halekas, P. R. Harvey, K. Issautier, J. C. Kasper, K. E. Korreck, V. K. Jagarlamudi, N. Lahmiti, D. E. Larson, A. Lecacheux, R. Livi, R. J. MacDowall, D. M. Malaspina, M. M. Martinović, N. Meyer-Vernet, M. Moncuquet, M. Pulupa, C. Salem, M. L. Stevens, Š. Štverák, M. Velli, and P. L. Whittlesey, Astrophys. J. Suppl. Series **246**, 62 (2020).
[52] V. Polito, J. Dudík, J. Kašparová, E. Dzifčáková, K. K. Reeves, P. Testa, and B. Chen, Astrophys. J. **864**, 63 (2018).
[53] K. Jockers, Astron. Astrophys. **6**, 219 (1970).
[54] J. Lemaire and M. Scherer, J. Geophys. Res. **76**, 7479 (1971).
[55] H. Lamy, V. Pierrard, M. Maksimovic, and J. F. Lemaire, Journal of Geophysical Research (Space Physics) **108**, 1047 (2003).
[56] M. Maksimovic, V. Pierrard, and J. F. Lemaire, Astron. Astrophys. **324**, 725 (1997).
[57] I. Zouganelis, M. Maksimovic, N. Meyer-Vernet, H. Lamy, and K. Issautier, Astrophys. J. **606**, 542 (2004).
[58] K. P. Dere, J. D. F. Bartoe, and G. E. Brueckner, Solar Physics **123**, 41 (1989).
[59] L. Teriaca, D. Banerjee, A. Falchi, J. G. Doyle, and M. S.

Madjarska, Astron. Astrophys. **427**, 1065 (2004).
[60] S. K. Tiwari, N. K. Panesar, R. L. Moore, B. De Pontieu, A. R. Winebarger, L. Golub, S. L. Savage, L. A. Rachmeler, K. Kobayashi, P. Testa, H. P. Warren, D. H. Brooks, J. W. Cirtain, D. E. McKenzie, R. J. Morton, H. Peter, and R. W. Walsh, Astrophys. J. **887**, 56 (2019).
[61] D. Berghmans, F. Auchère, D. M. Long, E. Soubrié, M. Mierla, A. N. Zhukov, U. Schühle, P. Antolin, L. Harra, S. Parenti, O. Podladchikova, R. Aznar Cuadrado, É. Buchlin, L. Dolla, C. Verbeeck, S. Gissot, L. Teriaca, M. Haberreiter, A. C. Katsiyannis, L. Rodriguez, E. Kraaikamp, P. J. Smith, K. Stegen, P. Rochus, J. P. Halain, L. Jacques, W. T. Thompson, and B. Inhester, Astron. Astrophys. **656**, L4 (2021).
[62] M. E. Molnar, K. P. Reardon, Y. Chai, D. Gary, H. Uitenbroek, G. Cauzzi, and S. R. Cranmer, Astrophys. J. **881**, 99 (2019).
[63] K.-S. Lee, H. Hara, K. Watanabe, A. D. Joshi, D. H. Brooks, S. Imada, A. Prasad, P. Dang, T. Shimizu, S. L. Savage, R. Moore, N. K. Panesar, and J. W. Reep, Astrophys. J. **895**, 42 (2020).
[64] N. E. Raouafi, G. Stenborg, D. B. Seaton, H. Wang, J. Wang, C. E. DeForest, S. D. Bale, J. F. Drake, V. M. Uritsky, J. T. Karpen, C. R. DeVore, A. C. Sterling, T. S. Horbury, L. K. Harra, S. Bourouaine, J. C. Kasper, P. Kumar, T. D. Phan, and M. Velli, Astrophys. J. **945**, 28 (2023).
[65] S. Serio, F. Reale, J. Jakimiec, B. Sylwester, and J. Sylwester, Astron. Astrophys. **241**, 197 (1991).
[66] K. Shibata and T. Magara, Living Reviews in Solar Physics **8**, 6 (2011).
[67] P. Antolin and C. Froment, Frontiers in Astronomy and Space Sciences **9**, 820116 (2022).
[68] J. C. Dorelli and J. D. Scudder, Geophys. Res. Let. **26**, 3537 (1999).
[69] M. Lazar and H. Fichtner, *Kappa Distributions: From Observational Evidences Via Controversial Predictions to a Consistent Theory of Nonequilibrium Plasmas*, Astrophysics and space science library (Springer, 2021).
[70] J. Candy and W. Rozmus, Journal of Computational Physics **92**, 230 (1991).